Modeling and Predictive Control of Shipboard Hybrid DC Power Systems

Daeseong Park, *Student Member, IEEE*, and Mehdi Zadeh, *Member, IEEE*

***Abstract*—Although onboard DC power systems bring values for the power and propulsion system of the future hybrid ships, the main barrier for the development of such systems for large scale vessels is the technical operational issues such as stability and power quality and how to satisfy the related standards and regulations. In the advanced ship power systems, the conventional diode rectifiers are being replaced with active front end (AFE) rectifiers providing the control flexibility but at higher cost. However, to make such devices more profitable, the ship control system can be reconfigured to unlock the potentials of AFEs for the general system stability. This paper is dealing with the stability issue of hybrid DC power systems proposing a predictive control approach to improve the voltage regulation and better use of converters. The proposed method replaces the conventional direct power control (DPC) of AFE rectifiers with a model predictive control (MPC) and integrates the DC-DC converters in the same control platform. In this method, optimal control commands for the rectifiers and the DC-DC converter are calculated by the predictive control to minimize the DC bus voltage fluctuations, especially under the fast load changes. The controller is then extended to regulate the load sharing between the different energy units. The effectiveness of the proposed method is evaluated in simulation with a typical ship load profile as well as a real ship profile which have several operating modes such as steep load increase & decrease, high speed, and maneuvering operation. The performance of the proposed control strategy is compared with conventional controllers, and the results show that the new method can provide significant advantages in terms of fast and stable control performance, as well as the steady-state voltage regulation and enhancing the power smoothing function of the battery. Laboratory experimental data are also used for validation.**

***Index Terms*—Model predictive control, batteries, onboard DC power system, hybrid electric ships.**

I. Introduction

Shipboard hybrid DC power systems have been raised as an alternative propulsion system in the marine industry recently [1]. Shipboard hybrid DC power system has advantages over the AC system concerning economical and environmental point of view because the diesel generators (DGs) can be operated with their optimal speed at the required load level. Then, the optimal operation reduces the fuel oil consumption of the ship, which leads to lower operating costs and emissions. Besides, the DC system can easily integrate energy storage systems (ESSs) such as batteries, supercapacitors, and fuel cells which are designed based on the DC system as shown in Fig. 1, which enables a cleaner and optimized sailing of the ship.

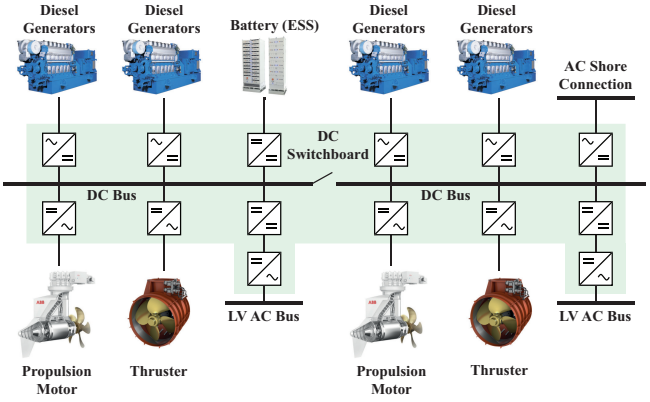

Fig. 1: A typical configuration of the shipboard hybrid DC power systems.

With the recent development of power electronics, the DC power system has become even more applicable with several research [2]–[5], and they have been installed for the small ferries. Catching up with this trend, the classification societies have come up with new regulations for the shipboard DC power systems. For example, the American Bureau of Shipping (ABS) has recently published the guidelines for DC power distribution systems for marine and offshore applications. Based on IEC 60092-101, the guideline recommends that the continuous voltage variations for DC distribution systems should be within $\pm 10\%$, and the ripple should be less than 10% . In abnormal conditions such as overcurrent, sudden load increase, load shedding (from equipment switching operations) and the transient overvoltage should be minimized so that other electrical components can withstand these voltage variations.

For the ships that sail long distances, the ships cannot be fully electrified by ESSs due to their lower energy density, so it requires huge weight and volume to install ESSs to cover such long distances. Therefore, it is still required to have DGs on board. As a result, the role and control strategies of the ESSs,

Manuscript received July 3, 2020; revised August 8, 2020; accepted September 22, 2020. (Corresponding author: Mehdi Zadeh)

The authors would like to thank the Research Council of Norway for financially supporting this work.

Daeseong Park and Mehdi Zadeh are with the Department of Marine Technology, Norwegian University of Science and Technology (NTNU), Trondheim, Norway (e-mail: daeseong.park@ntnu.no, mehdi.zadeh@ntnu.no).

as well as the power converters, should be discussed together. In the ship DC power system, there are available alternatives to choose a type of the rectifier, for example, diode or active front end (AFE) rectifier. With recent developments, AFE rectifiers have advantages over diode rectifiers such as controllable power factor, low harmonic input current, bidirectional power flow, etc. In this sense, AFE rectifiers should take main DC power sources converting AC power of the DGs and the main role of voltage regulation, while automatic voltage regulator of the generators keeps the AC voltage constant at the AC side.

To regulate the DC voltage by controlling the AFE rectifiers, control techniques are available based on pulse-width modulation (PWM). The most popular two different algorithms are voltage-oriented control (VOC) and direct power control (DPC). The comparative study of these two methods is presented in [6].

Model predictive control (MPC) is an advanced optimization based control technique, and significant research has been recently conducted to be applied in marine applications. A lot of MPC applications in the marine systems deal with power fluctuation smoothing with hybrid energy storage systems [7], DC-DC converter control for pulsed power load [8], [9], power and energy management [10], harmonic mitigation [11] and thrust control [12]. Not only in the marine application as a high-level control, but MPC has been also applied for the AFE rectifiers in order to regulate the DC voltage [13], [14]. The work in [13] shows DPC method that the predicted future states of currents and power of the AFE rectifier are used to control the active and reactive powers by selecting the optimal switching state within a finite control set. This is further extended, in [15], to show the fast and accurate tracking of dynamic DC voltage references. Based on the conventional predictive DPC method, there is some research to improve performance. A Lyapunov function is proposed for better stability and enhancing system performance reducing the computational time in [16]. The effect of the cost function is also studied by changing weighting factors dynamically in [17].

In the previous studies, a single energy source represented by one AFE rectifier with a resistive load is normally considered, and PI control method that comprises an inner (current) and outer (voltage) control loop is prevalently used for ESS control as a conventional method [18]. In the shipboard DC power systems, the tight control of the heavy power loads and switching operation between the multiple energy sources can cause serious DC voltage fluctuations which can result in a blackout in the entire power system, so the dynamic load profile should be considered as a constant power load (CPL). Moreover, it is necessary to consider the voltage regulation by several energy sources sharing the load among the DGs and the battery. In spite of the recent advancements, still a main issue in the system design and a main barrier for the development of the onboard DC power systems is the voltage stability especially under the load fluctuations and incorporating battery systems. These issues are not well addressed in the previous research.

This paper is dealing with the stability issues of onboard hybrid DC power systems with a general approach incorporating both low-level and high-level control design. To improve the general stability and voltage quality of the DC system, a control method is proposed which reduces the voltage fluctuations under different ship operating modes and especially transient loads. The controller is designed based on a predictive control approach and utilizes the capability of the existing converters for improving the system performance without additional equipment such as active/passive filters or DC choppers. The proposed controller incorporates the AFE rectifiers and the DC-DC converters at the same time for the maximum stabilizing effect. The control commands are generated by the MPC that minimizes the voltage fluctuation under the load variations and other influencing factors. This replaces the conventional DPC for the AFE rectifiers. The controller is extended to regulate the load sharing between the DGs and the battery by adding isochronous load sharing method and low-pass filters. Hence, the proposed MPC incorporates both the primary and the secondary controller in order to improve the performance of the ship power system. The performance of the proposed control strategy is compared with a conventional PI controller. The results show that the new method can provide significant advantages in terms of fast and stable control performance, as well as the steady-state voltage regulation and enhancing the power smoothing function of the battery. The laboratory experimental data are added for comparison.

TABLE I: Main Parameters of the Studied Onboard Power System

Parameter	Unit	Value
v_s	V	690
f_{ac}	Hz	60
R_s	mΩ	1
L_s	μH	10
R_{dc}	mΩ	1
L_{dc}	μH	3
C_{dc}	mF	50
$V_{dc,ref}$	V	1000
R_b	mΩ	1
L_b	μH	40
C_b	μF	400
$f_{sw,afe}$	kHz	20
$f_{sw,dc}$	kHz	10

The representative shipboard hybrid DC power system configuration is shown in Section II, and the dynamic modeling of the system is presented in Section III, as well as the control structure for both high-level and low-level controllers. The simulation is carried out with different cases and actual ship load profiles in Section IV, and the proposed controller is compared with an experimental case study in Section V. The conclusion of this study is explained in Section VI.

II. Shipboard Hybrid DC Power System

The electrical circuit diagram of the studied shipboard hybrid DC power system is presented in Fig. 2. The power system for the study consists of two three-phase generators (DG1 and DG2) with two AFE rectifiers, a DC link, a battery

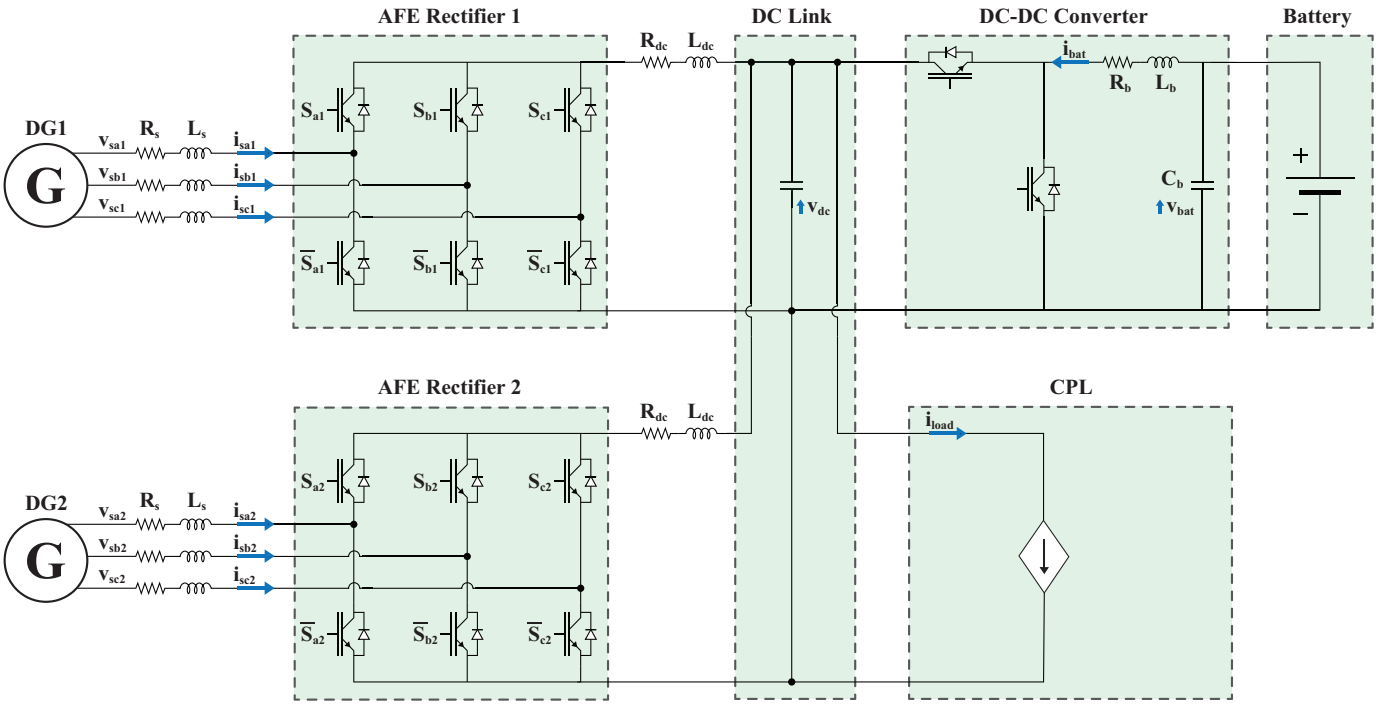

Fig. 2: Schematic diagram of the shipboard DC power system for the study.

bank with a DC-DC converter interface, and propulsion power loads which are summed and represented as CPL. It is assumed that the CPL includes a tightly regulated load converter and the associated propulsion motors. This is a reasonable assumption since the propulsion motors are controlled in constant power by variable speed drives (VSD). The parameters for the electrical components and equipment are listed in Table. I. For the simplification of the study, other resistive loads (e.g., hotel loads) are excluded from the consideration.

Also, a governor and an automatic voltage regulator (AVR) for the DG are omitted, so it is assumed that the AC voltage (v_s) and the frequency (f_{ac}) are kept stable during the simulation at 690V in root mean square (rms) value and 60Hz. As a result, the AC voltages of the DGs are independent of the load variations and the engine dynamics. In this work, the rectifiers are controllable, so the DC bus voltage is controlled by the AFE rectifiers, not by AVR from the AC side. Hence, the voltage set-points are given to the controllers of the rectifiers. Based on the set-points, each DG produces and supplies a share of the load power. The switching frequency of the AFE rectifiers ($f_{sw,afe}$) is 20 kHz at the maximum, and 10 kHz is used for the DC/DC converter control ($f_{sw,dc}$).

III. Dynamic Modeling of the System with Predictive Control

A. AFE Rectifiers with Predictive Control

The AFE rectifiers with six power transistors are shown in Fig. 2. Each AFE rectifier is connected to the three-phase voltage source V_s through the line filter inductances L_s and resistances R_s. The DPC by using predictive control is used to regulate the DC bus voltage (v_{dc}) as proposed in [13]. The voltages and currents of the three-phase system are transformed into $\alpha\beta$-frame as

$$v_{s1} = \frac{2}{3}(v_{sa1} + v_{sb1}e^{j(2\pi/3)} + v_{sc1}e^{j(4\pi/3)}) \quad (1)$$

$$i_{s1} = \frac{2}{3}(i_{sa1} + i_{sb1}e^{j(2\pi/3)} + i_{sc1}e^{j(4\pi/3)}) \quad (2)$$

The states of the two switches at each leg should be complementary to avoid short circuit (either "1" to be closed or "0" to be opened, respectively). Therefore, total of eight operation modes are expected to be considered as a finite-set constraint. The switching state vector and the AFE rectifier voltage are expressed in (3), and the resulting voltage vector of the AFE with v_{dc} is determined by the states of the switches as in (4).

$$S_{rec1} = \frac{2}{3}(S_{a1} + S_{b1}e^{j(2\pi/3)} + S_{c1}e^{j(4\pi/3)}) \quad (3)$$

$$v_{rec1} = S_{rec1}v_{dc} \quad (4)$$

The equations for the AFE rectifier 2 can be derived with the same procedure. The input current dynamics can be expressed for each AFE rectifier in the vector form as

$$L_s\frac{di_{s1}}{dt} = v_{s1} - v_{rec1} - R_s i_{s1} \quad (5)$$

$$L_s\frac{di_{s2}}{dt} = v_{s2} - v_{rec2} - R_s i_{s2} \quad (6)$$

With the measured powers from the battery (P_{bat}) and the CPL (P_{load}), the voltage equation at the DC link can be described as

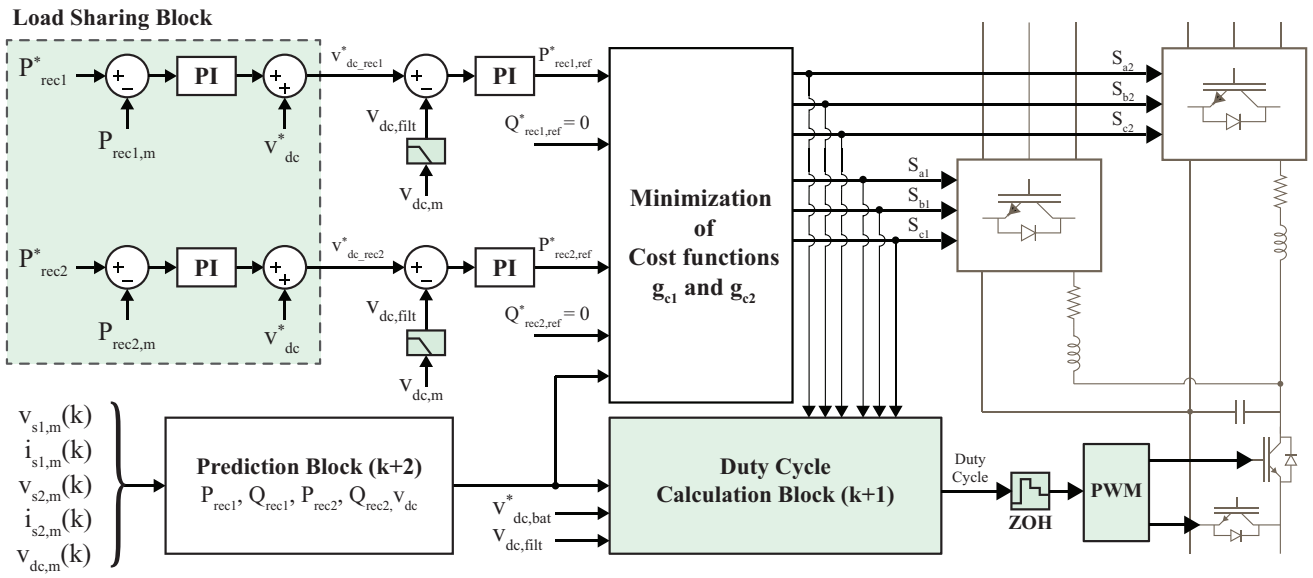

Fig. 3: The control strategy for the AFE rectifiers with load sharing logic and the DC-DC converter by using model-based predictive control.

$$C_{dc}\frac{dv_{dc}}{dt} = S_{rec1}i_{s1} + S_{rec2}i_{s2} + \frac{P_{bat,m}}{v_{dc}} - \frac{P_{load,m}}{v_{dc}} \quad (7)$$

Due to the high switching frequency and the simplicity of the model of the AFE rectifiers, it is sufficient to use forward Euler approximation for the discretization. The predicted input current in (5)-(6) and the DC bus voltage in (7) becomes

$$i_{s1}(k+1) = \Big(1 - \frac{R_s T_s}{L_s}\Big) i_{s1}(k) + \frac{T_s}{L_s}\Big(v_{s1}(k) - v_{rec1}(k)\Big) \quad (8)$$

$$i_{s2}(k+1) = \Big(1 - \frac{R_s T_s}{L_s}\Big) i_{s2}(k) + \frac{T_s}{L_s}\Big(v_{s2}(k) - v_{rec2}(k)\Big) \quad (9)$$

$$v_{dc}(k+1) = v_{dc}(k) + \frac{T_s}{C_{dc}}\Big(S_{rec1}(k)i_{s1}(k) + S_{rec2}(k)i_{s2}(k) + \frac{1}{v_{dc}(k)}(P_{bat}(k) - P_{load}(k))\Big) \quad (10)$$

Similarly, the $(k+2)$th instant can also be calculated. With kth measured states, each eight $i_{s1}(k+2)$, $i_{s2}(k+2)$ and $v_{dc}(k+2)$ can be estimated based on each switch state candidate of $S_{rec1}(k+1)$ and $S_{rec2}(k+1)$. The input voltages in the AC grid, v_{s1} and v_{s2} at $(k+1)$ and $(k+2)$th instants, are estimated with the angle of the voltage vector according to the angular frequency of the AC grid voltage and the sampling interval. Because the AC frequency is assumed to be constant, the use of phase-locked loop (PLL) is not considered in the modeling to detect the system frequency. The predicted instantaneous active power and reactive power of the AFE rectifiers are described as

$$P_1(k+2) = Re(v_{s1}(k+2)\bar{i}_{s1}(k+2)) \quad (11)$$

$$Q_1(k+2) = Im(v_{s1}(k+2)\bar{i}_{s1}(k+2)) \quad (12)$$

$$P_2(k+2) = Re(v_{s2}(k+2)\bar{i}_{s2}(k+2)) \quad (13)$$

$$Q_2(k+2) = Im(v_{s2}(k+2)\bar{i}_{s2}(k+2)) \quad (14)$$

The optimal switching states are determined based on the calculation of the cost functions with the weighting factors K_{ij} $(i = 1, 2, 3)$ and $(j = 1, 2)$ as

$$g_{c1} = K_{11}|P_{rec1,ref} - P_1(k+2)| + K_{21}|Q_{rec1,ref} - Q_1(k+2)| + K_{31}|v_{dc,ref} - v_{dc}(k+2)| \quad (15)$$

$$g_{c2} = K_{12}|P_{rec2,ref} - P_2(k+2)| + K_{22}|Q_{rec2,ref} - Q_2(k+2)| + K_{32}|v_{dc,ref} - v_{dc}(k+2)| \quad (16)$$

The normalization of the voltage, active and reactive powers are not applied in the calculation of the cost function. Instead, tuning work of the weighting factors is carried out.

B. Load Sharing Between the Energy Sources

In the shipboard hybrid DC power system, load sharing between the AFE rectifiers can be done by the DC voltage droop control which is similar to the well-known frequency droop in AC systems. However, when the droop (i.e. the slope of the droop curve) is zero, it becomes isochronous mode load sharing. In this work, the isochronous mode is used. The voltage set-points of the AFE rectifiers change with PI controller with a dominant proportional gain to follow each load reference close to a linear curve, but it aims to maintain the constant DC voltage reference of 1000V. This is because to eliminate the influence of the voltage fluctuation from the

droop control and to test the system having different sizes of the DGs in addition to their unequal load sharing. The reference voltage from the load sharing block for the AFE rectifiers increases when the load reference is increased (i.e., the DG should generate more power) and vice versa. The block diagram including the predictive control and the load sharing functions for the DGs and associated AFE rectifiers is shown in Fig. 3. Since the voltage reference of the battery does not change and set to $v_{dc,ref}$ as well, the battery is also operated in the isochronous mode which only compensates the transient loads as a swing machine [19], [20]. To assign fast load compensation to the battery and slow transient to the DGs, low-pass filters are used in the DC voltage measurement as seen in Fig. 3, because the fast transient from the DGs can cause voltage/frequency fluctuations and faster wear out of the mechanical components.

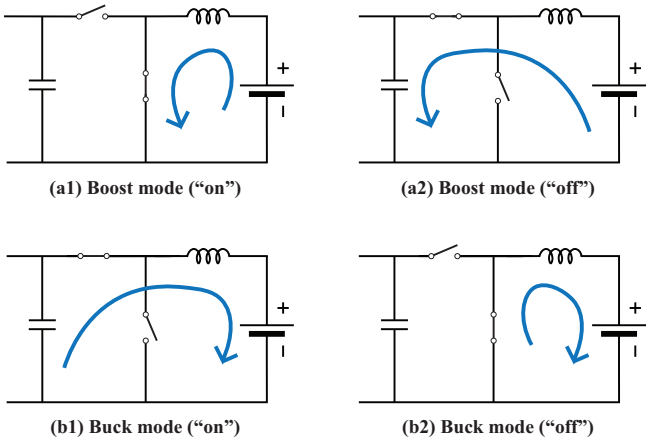

Fig. 4: The control of the switches in the DC-DC converter for boost and buck mode.

C. DC-DC Converter

In the marine applications, a half-bridge bidirectional with multiple current paths or an isolated full-bridge bidirectional DC-DC converter can be used to integrate the battery to the DC link. For a full-bridge bidirectional DC-DC converter, a high-frequency transformer is used for changing the voltage level and providing the galvanic isolation for safety [21]. In this study, the half-bridge topology is used as it is used prevalently in the industry [22]. However, the multiple current paths are simplified into one for the modeling as shown in Fig. 2.

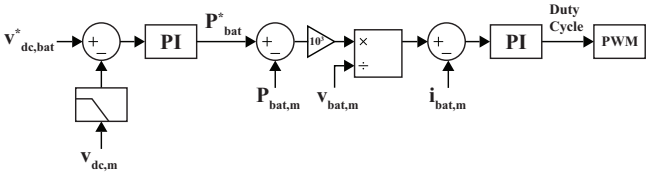

Fig. 5: PWM generation to control the DC-DC converter switches by using PI controllers. (the subscript "m" is used for the measured signal)

The current from the battery i_{bat} has a positive sign for battery discharging and negative sign for charging. Since the DC-DC converter is modeled to have a bidirectional mode, two switches are controlled as shown in Fig. 4. For the simplicity of the model, the resistance R_b is neglected because R_bT_s is a very small value in the modeling.

With a conventional PI controller, the battery power is regulated by the DC-DC converter to smoothen the DC bus voltage as shown in Fig. 5. The reference inductor current is calculated by dividing the battery power reference by the battery voltage. The battery power reference is derived from PI controller by using the DC bus voltage error, and this error is calculated from $v_{dc,bat,ref}$ which can be set for the load sharing.

As an alternative controller proposed by this paper as shown in the duty cycle calculation block in Fig. 3, the predicted $v_{dc}(k+2)$ in (10) can be filtered and used to control the DC-DC converter by calculating $i_{bat,ref}(k+1)$ to compensate the voltage deviation from the battery output voltage reference ($v_{dc,bat,ref}$) given by the high-level controller in (18) as

$$\begin{aligned} v_{dc,filt}(k+2) =& v_{dc,filt}(k+1) + \frac{T_s}{C_{dc}}\Big(S_{rec1}(k+1)i_{s1}(k+1) \\ &+ S_{rec2}(k+1)i_{s2}(k+1) \\ &+ \frac{1}{v_{dc,filt}(k+1)}(P_{bat}(k) - P_{load}(k))\Big) \end{aligned} \tag{17}$$

$$\begin{aligned} i_{bat,ref}(k+1) =& i_{load}(k+1) + \frac{C_{dc}}{T_{s,bat}}\Big(v_{dc,bat,ref}(k) \\ &- v_{dc,filt}(k+2)\Big) - \Big(S_{rec1}(k+1)i_{s1}(k+1) \\ &+ S_{rec2}(k+1)i_{s2}(k+1)\Big) \end{aligned} \tag{18}$$

In the simulation for both methods, $v_{dc,bat,ref}$ is equal to $v_{dc,ref}$. The current reference is calculated based on the filtered v_{dc} to assign less stress on the battery. The time constant of the filter should be chosen carefully because bigger value leads to a slower response for tracking the power reference during the load changes while too small constant can produce voltage instability during the high load condition. At each mode, the current equations of the DC-DC converter can be modeled and discretized with duty cycle d and the sampling time $T_{s,bat}$(=100 μs), (19) for buck mode and (20) for boost mode as

$$i_{bat}(k+1) = i_{bat}(k) + \frac{T_{s,bat}}{L_b}(d(k)v_{dc}(k) - v_{bat}(k)) \tag{19}$$

$$i_{bat}(k+1) = i_{bat}(k) + \frac{T_{s,bat}}{L_b}(v_{bat}(k) - (1 - d(k)v_{dc}(k)) \tag{20}$$

Then, the duty cycles at $(k+2)$th instance for each mode of operations, (21) for buck mode and (22) for boost mode, can be calculated by setting $i_{bat}(k+2) = i_{bat,ref}$ as

$$\begin{aligned} d(k+1) =& \frac{1}{v_{dc}(k+1)}\Big\{\frac{L_b}{T_{s,bat}}\Big(i_{bat,ref}(k+1) - i_{bat}(k+1)\Big) \\ &+ v_{bat}(k+1)\Big\} \end{aligned} \tag{21}$$

$$\begin{aligned} d(k+1) =& \frac{1}{v_{dc}(k+1)}\Big\{\frac{L_b}{T_{s,bat}}\Big((i_{bat,ref}(k+1) - i_{bat}(k+1)\Big) \\ &- v_{bat}(k+1) + v_{dc}(k+1)\Big\} \end{aligned} \tag{22}$$

However, the duty cycle should be imposed by a lower and upper limit between 0 and 1 after the calculation above.

D. Battery

Li-ion battery model developed by [23] is used in this study. However, the effects of the temperature and aging are not considered in the equation for this study. The mathematical equations for discharge (23) and charge (24) are given as

$$V_{batt,dcg} = E_0 - R\cdot i - K\left(\frac{Q}{Q-\int_0^t idt}\right)\cdot\left(\int_0^t idt + i^*\right) + Ae^{-B\times\int_0^t idt} \quad (23)$$

$$V_{batt,cg} = E_0 - R\cdot i - K\left(\frac{Q}{\int_0^t idt - 0.1Q}\right)i^* - K\left(\frac{Q}{Q-\int_0^t idt}\right)\cdot\int_0^t idt + Ae^{-B\times\int_0^t idt} \quad (24)$$

where,

V_{batt}= battery voltage (V)
E_0= battery constant voltage (V)
K= polarisation constant (V/Ah) or resistance (Ω)
Q= battery capacity (Ah)
$\int idt$= actual battery charge (Ah)
A= exponential zone amplitude (V)
B= exponential zone time constant inverse $(\text{Ah})^{-1}$
R= internal resistance (R)
i= battery current (A)
i^*= filtered battery current (A)

The battery parameters are chosen as listed in Table. II. According to the sizing of the battery, it can produce 325 kW at 1C rate (for an hour). However, the operation of the battery is limited to 3C rate for discharging and 2C rate for charging in the simulation, since the C-rate is normally controlled to limit the temperature increase and the degradation in the reality.

TABLE II: Battery Model Parameters

Parameter	Unit	Value
E_0	V	650
Q	Ah	500
K	Ω	0.009
A	V	50.39
B	Ah^{-1}	0.1221
R	Ω	0.012

E. Load as Constant Power Load

Since the major part of the load is the propulsion load that is tightly controlled at constant power, the required loads are summed up and modeled as CPL seen from the DC link. Then, the load model is represented as a controlled current source with PI controller to follow the load reference.

IV. Results and Discussions

To verify the performance of the proposed control strategy, simulation models are established and used for the dynamic analysis of the system. The simulations are performed in Matlab/Simulink software with the switching model of the converters. Simulation cases can be divided into two scenarios, the first scenario without battery operation and the second scenario with battery operation. Without battery operation, the simulation is carried out to check the performance of the AFE rectifiers with different load profiles, prediction functions, and cost function parameters. With battery operation, the effects of the battery operation are observed by changing the control method, and the load sharing performance between the DGs and the battery bank is presented. The performance of the proposed controller is compared with the conventional PI controller.

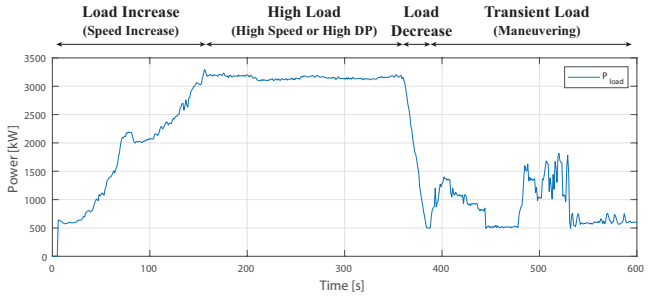

Fig. 6: Ship load profile modeled as a constant power load.

To validate the effectiveness of the proposed controller, different load profiles are tested; first, a simple step-wise load profile is tested, and secondly, the controller is tested under the operational profile of a ship. This load profile is drawn based on the measured data from the real operation of the vessel, as shown in Fig. 6. In this profile, from the beginning to 150s, the load is constantly increasing as the ship speed increases, and the high speed or high load of dynamic positioning (high DP with zero speed) is kept until 380s. Then, the load (ship speed) decreases instantly to start maneuvering operation near the harbor (or the destination). The simulation results are filtered for better visibility.

A. First Scenario: without Battery Operation

First, the performance of the predictive control strategy is tested with step-wise load power variations as shown in Fig. 7. At the same time, the weight factor, K_3, is varied to observe its effect. In the figure, the red line represents the DC bus voltage set-point fixed at 1000 V. The resulting DC bus voltages are indicated with different values of K_3, and the grey dashed lines show the standard limit of the voltage defined by the ABS rules.

It is observed that the voltage oscillates with the load changes. As shown in the figure, the proposed controller is able to regulate the DC voltage at the reference value. The DC bus voltage is within the acceptable range for most of the load level and the load change. However, the peak of the oscillations exceeds the limit when the load change is

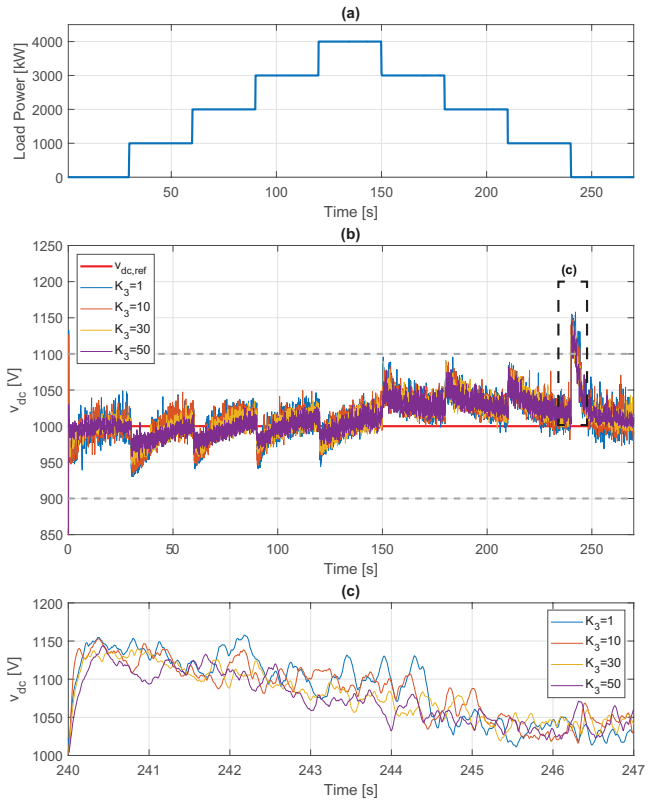

Fig. 7: The performance test of the controller for voltage regulation under the step-wise load variation with different weighting factors for DC bus voltage in the cost function ($K_1 = 1$ and $K_2 = 1$) (a) Step-wise Load Power (b) DC bus voltage (c) DC bus voltage (enlarged).

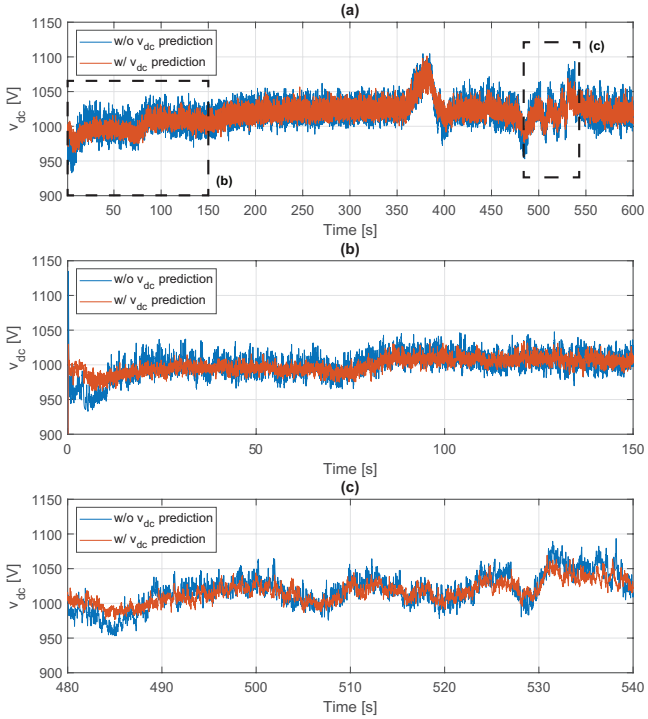

Fig. 8: Comparison with and without DC bus voltage prediction in the predictive control strategy (without battery operation). (a) DC bus voltage. (b) DC bus voltage in load increase operation. (c) DC bus voltage in maneuvering operation.

significantly high, e.g., when the load power is stepped down to no load. However, there is a minimum load limitation such as ramp rate from the DGs, so these peaks can be usually avoided during the actual operation.

The control performance including v_{dc} prediction is dependent on the weighting factors in the cost function in (15) and (16). Since the parameters in the cost function are not normalized, the weighting factors for the active power (K_1) and reactive power (K_2) are kept at unity, and the weighting factor for the voltage (K_3) is only varied. The result is shown in Fig. 7. As K_3 increases, the fluctuation level and the overvoltage are slightly reduced as seen in 7 (b) and (c), and the performance of the controller maintains this trend in general until around $K_3 = 50$. However, with higher values of K_3 over 60, the voltage instability at the high load is observed. Based on trial and error as described, the optimal value for K_3 to meet the stable operation is identified and chosen as $K_3 = 50$.

In the next step, the simulation is carried out with the actual load profile as explained in Fig. 6, and the results are shown in Fig. 8. The biggest transient overvoltage can be observed at around 380s when the load is suddenly decreased from around 3200kW to 500kW, and the biggest undervoltage can be found at around 10s when the load is increased from no-load condition to 600kW. The voltage at the initial stage is enlarged as seen in Fig. 8 (b), and with v_{dc} prediction, it is observed that the undervoltage and the fluctuation level are reduced. Also, the voltage fluctuates as the load changes rapidly for the ship maneuvering operation. The voltage in this range can be seen closely in Fig. 8 (c). Comparing with the result without v_{dc} prediction function (i.e., without (10)), the voltage returns faster to the set-point value (1000V) with v_{dc} prediction function, and the voltage peaks are reduced during the load changes afterward. The standard deviation is calculated to compare the voltage deviation from the set-point for both conditions. The result shows a clear improvement of the voltage fluctuation by 58.1711 for without v_{dc} prediction and 46.4419 for with v_{dc} prediction.

B. Second Scenario: with Battery Operation

In the second scenario, the battery is connected to the DC link through the DC-DC converter by including PI controller in Fig. 5 and the predictive control method in (18) – (22) as they are different cases while the AFE rectifiers still have MPC.

The results of these control strategies for the DC-DC converter are presented in Fig. 9 with 80% of the initial state of charge (SoC) of the battery. With PI control, the voltage ripple is slightly reduced compared to the result without battery operation. At the high load condition, the battery tries to correct the voltage to the reference, but the undershoot occurs due to the slow dynamics of the battery control. From 400s, the voltage ripple becomes greater and the voltage peaks are not so much reduced at the maneuvering operation mode.

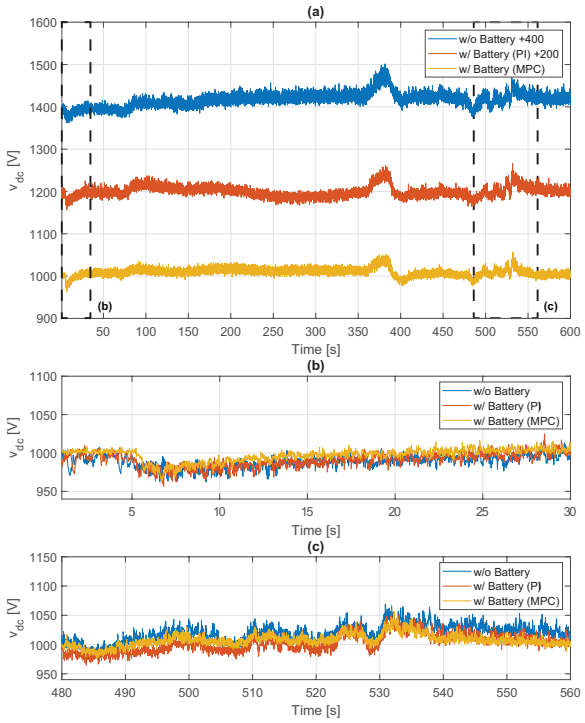

Fig. 9: The performance comparison of the DC bus voltage with different control methods for the DC-DC converter. (MPC for the AFE rectifiers) (a) Whole operation (b) Load increase operation (c) Maneuvering operation

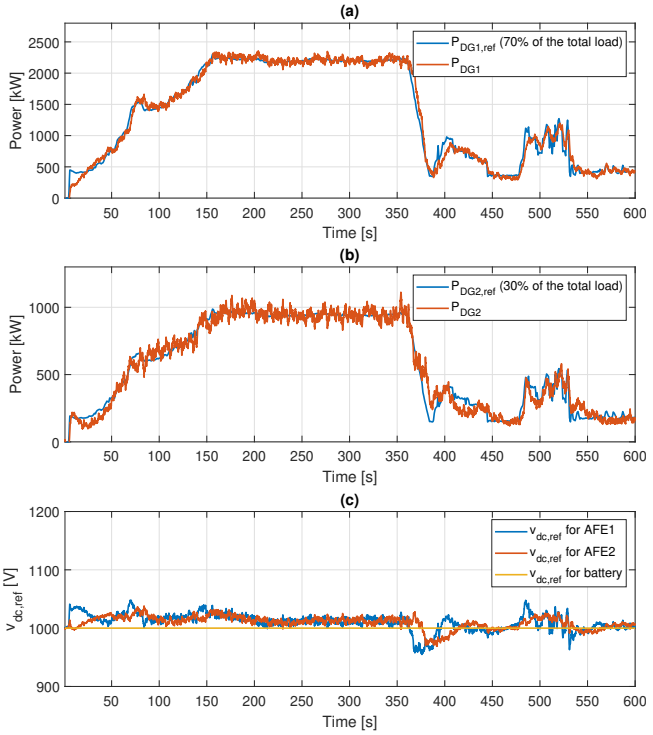

Fig. 10: The load sharing between the DGs with the voltage control. (a) The power supplied by the DG 1 through the AFE rectifier 1. (b) The power supplied by the DG 2 through the AFE rectifier 2. (c) Reference voltage for each rectifier and the battery converter during the load sharing

With the predictive control strategy, the performance of the voltage regulation is much better overall. The voltage peaks due to the load changes are significantly reduced, and the amplitude of the voltage ripples is also reduced. The slow-varying voltage fluctuation at the high load to correct steady-state voltage error is eliminated, and the overvoltage at around 380s is much more reduced. In addition, the voltage is more stabilized during the maneuvering operating mode. The voltage deviations as a standard deviation from the reference voltage of 1000V are calculated as given in Table. III. As same as the observation from Fig. 9, the amplitude of the voltage ripple of the predictive method is reduced by 24.1% from the case without battery operation and 3.8% from the case with PI control.

TABLE III: Standard deviation of v_{dc} from the reference of 1000 V

Control method	Standard Deviation
without Battery	46.4419
with Battery (PI)	36.6610
with Battery (MPC)	35.2724

Besides, the load sharing between the DGs is presented in Fig. 10. The power measurements are filtered for the sake of visibility. Since the optimal load sharing between the DGs is out of the scope of this work, each load percent is assigned unequally with the fixed rate at 70% for the DG1 through AFE rectifier 1 and 30% for the DG2 through AFE rectifier 2 of the total load to consider even unequal sizes of the DGs.

In Fig. 10 (a) and (b), the results show that the DGs supply the power through the AFE rectifiers according to the reference, but there are some deviations during the load variations. For example, the DG2 provides more power than the reference during $375-400$s, and the deviation starts for both DGs from this point. This can be understood as seen in Fig. 10 (c) that the deviation becomes larger when the sign of the rate of the voltage set-point for the rectifiers is different (i.e. when the voltage set-points cross each other).

In Fig. 11, the indirect result of the proposed controller for the power smoothing (peak-shaving) performance by the battery is presented with the predictive control method. When the powers supplied from the DGs are summed, there is a gap between the supplied power by the DGs and P_{load} as seen in Fig. 11 (b) (green area) which presents the most effective performance especially at maneuvering operation during $350-550$s. As intended, this power gap is supplied by the battery as seen from the battery power in Fig. 11 (c). When the result is compared to the case without the battery (i.e. P_{load}), the power supplied from the DGs through the AFE rectifiers are smoothened by the battery acting as a peak shaving mode, so that the DGs can be operated at more stable and slow-varying conditions. This battery control strategy does not intend for the battery to be performed as a load levelling mode, so Fig. 11 (d) shows that the SoC of the battery does not change significantly during the whole time of operation.

The averaged switching frequencies for both AFE rectifiers

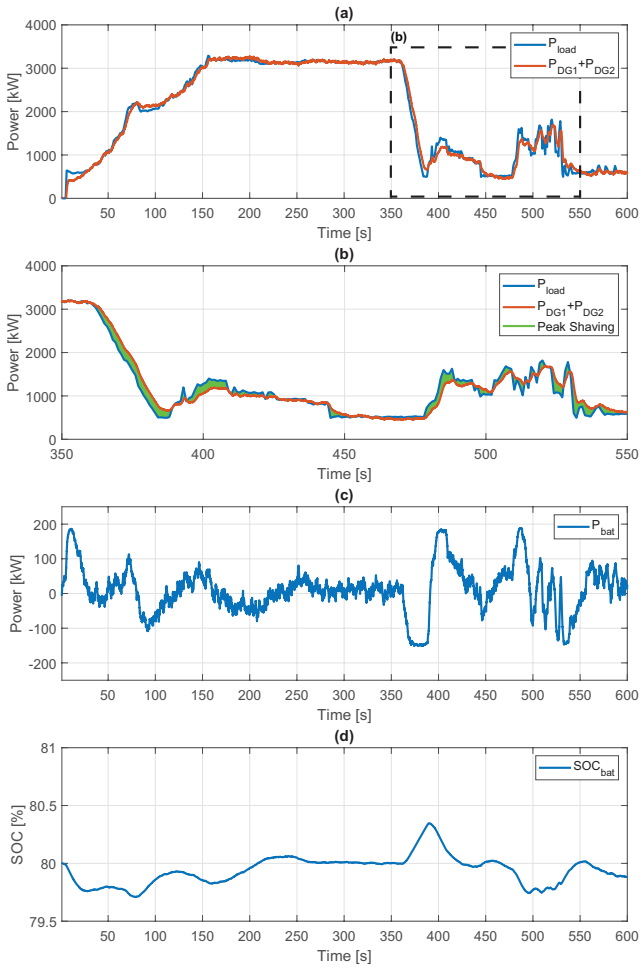

Fig. 11: The performance of the DC-DC converter and the battery for the power smoothing. (a) Supplied power by the DGs through the AFE rectifiers with the battery operation. (b) Peak-shaving operation by the proposed control method (c) Supplied/consumed power by the battery. (d) SoC of the battery

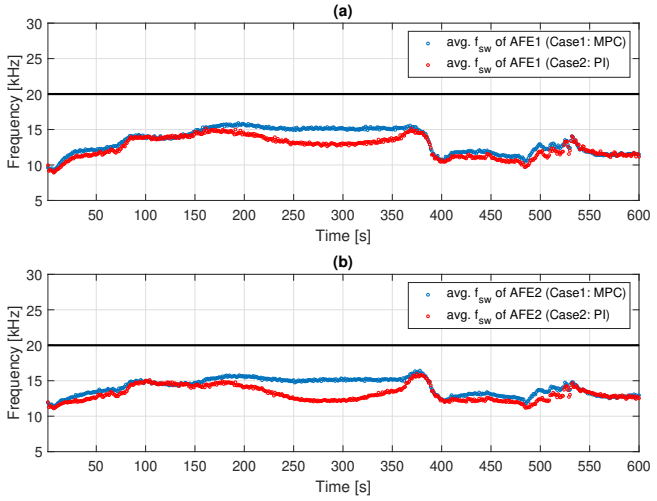

Fig. 12: The averaged switching frequency of AFE rectifiers for the comparison when the different control methods (MPC and PI) is applied to the DC-DC converter (a) AFE rectifier 1 (b) AFE rectifier 2

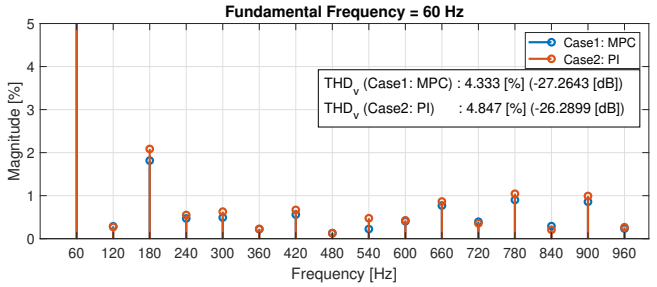

Fig. 13: The comparison of the total harmonic distortion at the AC side voltage with 60 Hz of the fundamental frequency (Case1: MPC for both AFE rectifiers and DC-DC converter, Case2: MPC for AFE rectifiers, PI control for DC-DC converter)

are presented in Fig. 12. The maximum switching frequency is 20kHz, but its average is calculated every 1s by counting changes of the switching state of the AFE rectifier. Then, it is divided by the total number of instants. As seen in Fig. 11, the better performance costs higher averaged switching frequency of MPC than that of PI control method, but it is still under the maximum switching frequency.

Total harmonic distortion (THD) of A-phase input voltage for AFE rectifier1 is also compared in Fig. 13 for both two control cases. As per the regulation from IEEE (IEEE Std 45.1-2017, IEEE Recommended Practice for Electrical Installations on Shipboard Design), the voltage THD should be no more than 8% with no single voltage harmonic exceeding 5%. Since the AFE rectifier is used with 20kHz of its maximum switching frequency, the calculations and measurements take into consideration harmonics up to the 100th order (but presented in the figure up to the 20th order). The result shows that the AC voltage THD is improved by 10.61% with the proposed method by the effort to stabilize the DC voltage with the DC-DC converter through MPC. This reflects the mutual effect between the DC bus stabilization and the THD of AC side.

Lastly, even a higher transient load profile based on a real ship load data (from an offshore supply vessel) is tested as shown in Fig.14 (a) to investigate the dynamic performance of the proposed controller. The result of v_{dc} is presented in Fig. 14. Similar to the earlier results in Fig. 9, the results show that the proposed method can keep the voltage more stable at the set-point and the fluctuations are much more reduced in case of the proposed method (Case1: MPC) than the conventional control method (Case2: PI control for DC-DC converter).

To sum up, the regulation of the DC bus voltage can be improved by the prediction of the future states of the DC bus voltage and the integration of the battery. By assigning the constant voltage set-point to the DC-DC converter control, the battery can be performed as a voltage/power peak shaving mode. Especially, the significant difference is observed at the high load condition to maintain v_{dc} constant at the set-point.

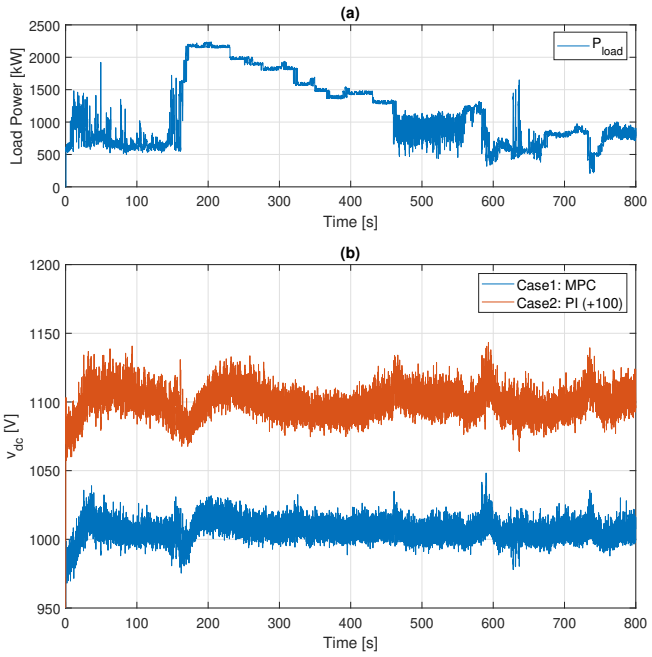

Fig. 14: The dynamic performance test with a high transient load profile (a) Load Profile (b) v_{dc} (Case1: MPC for both AFE rectifiers and DC-DC converter, Case2: MPC for AFE rectifiers, PI control for DC-DC converter)

V. Experimental Validation

The proposed control method is compared with a set of experimental results collected from the hybrid power lab in Norwegian University of Science and Technology (NTNU) [24] [25]. The configuration of the test-bed is shown in Fig. 15. There are two sets of diesel engines and generators with rectifiers, and batteries which are connected to DC-bus through DC-DC converters. Two electric motors with brakes can be used to emulate the propulsion load of the marine vessels. The motor loads are controlled by variable speed drives (VSDs) given by speed and torque reference to shape the ship load profile.

TABLE IV: Specifications of the Test-bed [24], [25]

Equipment	Specifications
Diesel Generator	400 kVA, 4 poles, 1500 rpm
Battery Bank	Li-ion, 65 Ah, 346 V
Electric motor loads	160 kW, 1,015 nm at 1500 rpm
DC Bus Voltage	560 V

Detail specifications of the equipment can be found in Table. IV. The load profile has three segments meaning different types of operations, and they are tested separately. Each segment is called Mode 1, 2, and 3 as shown in Fig. 17.

The proposed control design is compared with the experimental data collected from the hybrid power system running with ABB power management system. In order to assimilate the simulation and the laboratory setup, the control parameters such as droop gains are tuned in the simulation based on Equivalent Consumption Minimization Strategy (ECMS) approach in [24]. However, there are still differences between

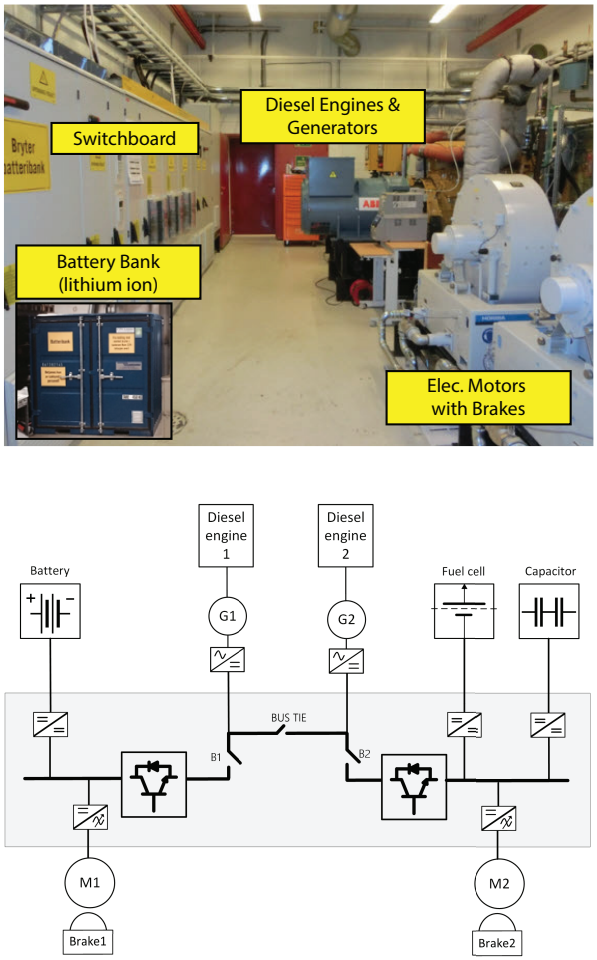

Fig. 15: Laboratory facility in Hybrid Power Lab (a) Equipment Installation (b) Single Line Diagram of the Lab

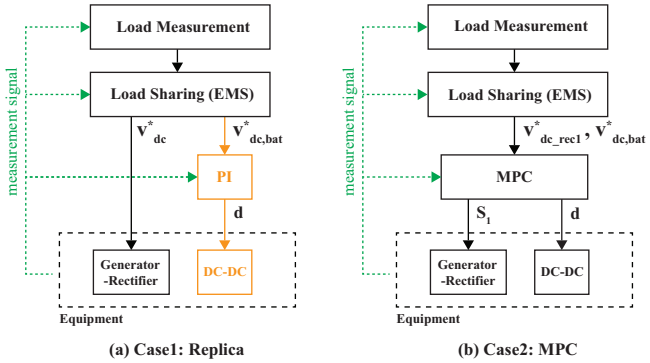

Fig. 16: The process diagram for the comparison of the control structures between the two different cases

the simulation and the experimental set-up mainly due to the low-level control system of the converters in the laboratory. Also, the laboratory set-up cannot be fully accessible to be replicated in the simulation model. Besides, some passive components like filter inductors and capacitors are simplified in the simulation model which makes the model a bit different from the experimental set-up.

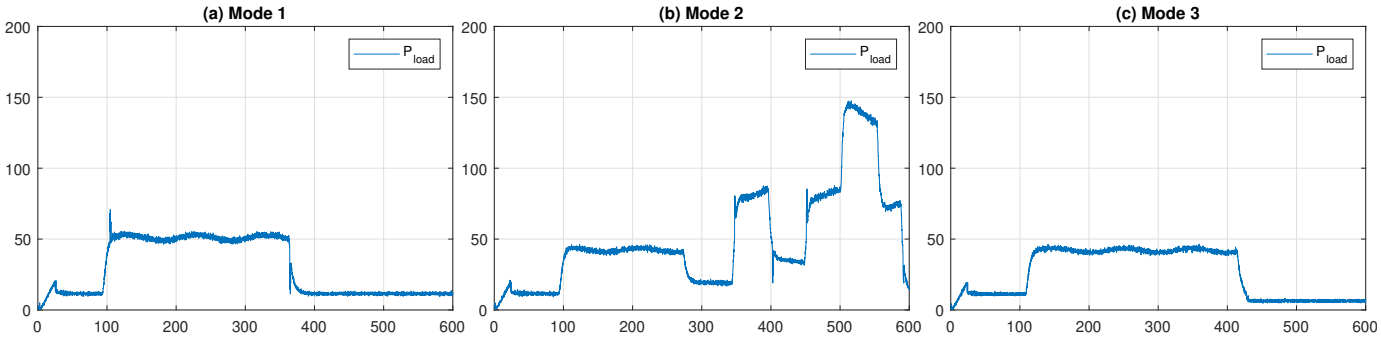

Fig. 17: Three different load profiles of P_{load} $[kW]$ (a) Mode 1, (b) Mode 2, (c) Mode 3

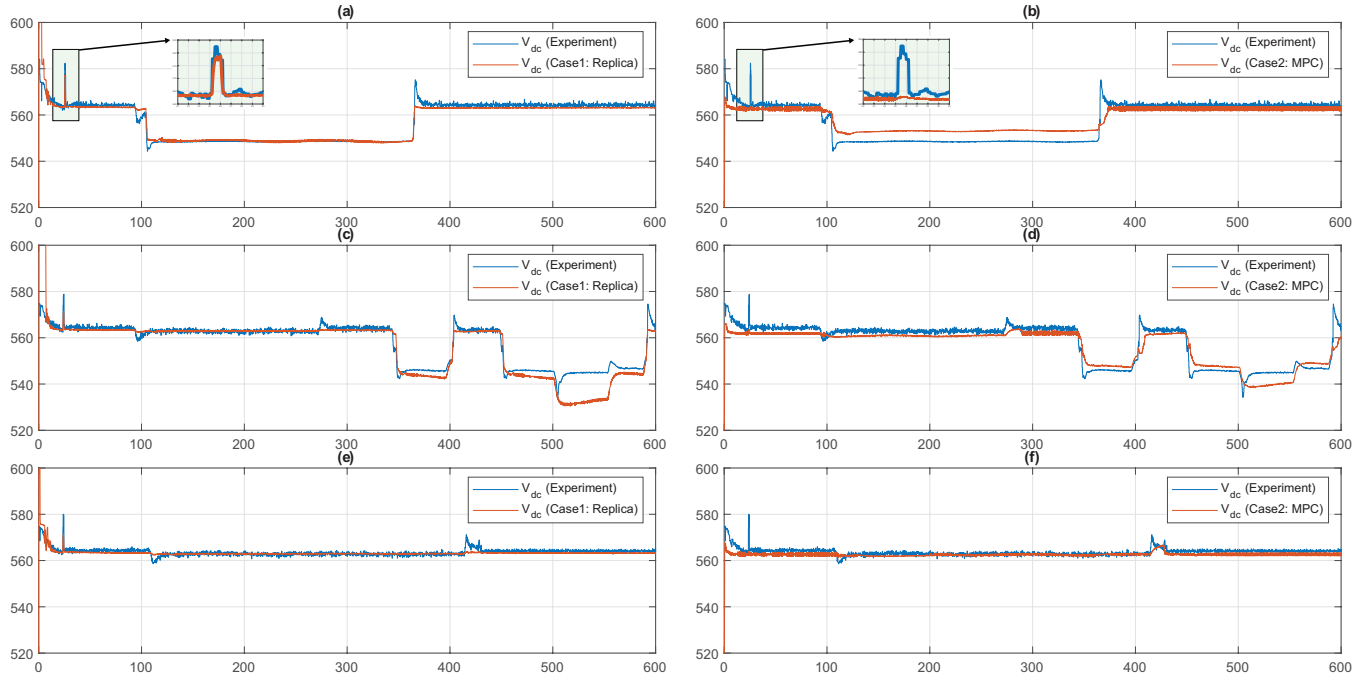

Fig. 18: Comparison between the experiment and the simulation (Case 1: Replica and Case 2: MPC) for $v_{dc}[V]$ (a, b) Mode 1 (c, d) Mode 2 (e, f) Mode 3

There are two scenarios for the simulation to compare the results with the experimental results. One case is a simulation model as a replicated experimental set-up (Case 1: Replica), and the other case is made by replacing the converter controllers with the proposed controller (Case 2: MPC). The processes of these two different control structures are compared in Fig. 16. Case 1 matches better with the experimental results since it is replicating the laboratory although Case 2 shows a better performance under the transient behavior.

In Fig. 18 & 19 (a), (c), and (e), the results of v_{dc} and P_{bat} show the simulation results based on Case 1 are valid as they are compared with the experimental results. Then, it is presented that the proposed controller shows improved performance in the voltage regulation in Fig. 18 (b), (d), and (f) by applying the same load profile. For the simulation of Case 2, the dc voltage reference for the MPC calculation block is given following the experimental result to include voltage droop function. Therefore, only the difference between the control methods (PI versus MPC) can be seen in the results.

As expected in the simulation study in Chapter IV, the proposed controller should be able to handle fast transient and peaks in the voltage control and to smoothen rapid voltage variations by adjusting the battery power automatically. When v_{dc} from the simulation results based on Case 2 is compared with the experimental results, the major benefit is to eliminate the voltage spike at approx. 25s for all the modes of the load profile. The voltage spike is observed in the experimental and Case 1 results due to the sudden load decrease, resulting in approx. 15V of the spike, but the proposed controller can manage to minimize the voltage spikes. In addition, by the battery power control of the proposed controller (Case 2), rapid changes in the DC voltage has been mitigated as seen in 370s in Fig. 18 (b) and $350 - 600$s in Fig. 18 (d).

The proposed control method has a voltage compensation function by the battery. This function is realized by assigning reference battery current in consideration of the voltage control as specified in (18). Therefore, the charging/discharging power of the battery should be determined accordingly. As seen in

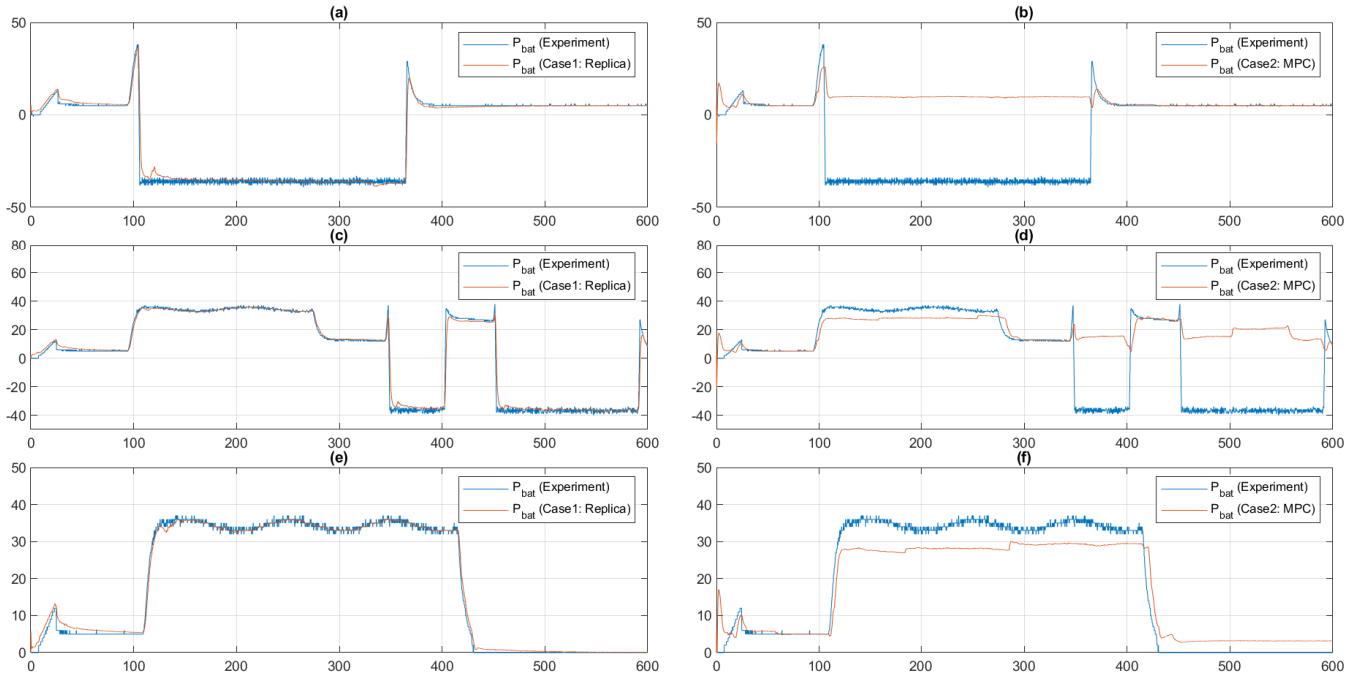

Fig. 19: Comparison between the experiment and the simulation (Case 1: Replica and Case 2: MPC) for the battery power, P_{bat} $[kW]$ (a, b) Mode 1 (c, d) Mode 2 (e, f) Mode 3

Fig. 19 (b), (d), and (f), the battery behaves differently from the experiment and Case 1. As a result, sudden spikes of charge and discharge of the battery is avoided while the generator set and the battery supply the same required load.

VI. Conclusion

In this paper, a control system is proposed to mitigate the DC voltage fluctuations and transients in the shipboard hybrid DC power systems. This controller is designed based on the predictive control approach and encompasses both the primary and secondary control layers. The proposed controller replaces the conventional DPC which is used in marine power systems for the regulation of rectifiers and DC-DC converters. The controller is extended to control the DC-DC converter of the battery interface at the same time and to regulate the load sharing between the DGs and the battery. Therefore, the predictive control approach is contributing to both primary and secondary control of the DC power system.

The simulation and the comparison with the experimental results show the effectiveness of the proposed method to regulate the DC bus voltage providing much faster dynamics and stable operation. This is important to meet the rules and standards for onboard power systems. If the battery is used for power smoothing as proposed in this paper, the SoC does not vary significantly while the DC bus voltage can be stabilized at a constant level. Therefore, the proposed method improves the general stability of the power system as well as the lifetime of the battery. The results show that the switching frequency of the AFE rectifiers can remain in the controllable range. The comparison between the experimental and the replicated simulation results show not only its fidelity of the modeling but also the effectiveness of the proposed controller.

References

[1] P. Ghimire, D. Park, M. K. Zadeh, J. Thorstensen, and E. Pedersen, "Shipboard Electric Power Conversion: System Architecture, Applications, Control, and Challenges [Technology Leaders]," *IEEE Electrification Mag.*, vol. 7, DOI 10.1109/MELE.2019.2943948, no. 4, pp. 6–20.

[2] M. K. Zadeh, R. Gavagsaz-Ghoachani, J.-P. Martin, S. Pierfederici, B. Nahid-Mobarakeh, and M. Molinas, "Discrete-Time Tool for Stability Analysis of DC Power Electronics-Based Cascaded Systems," *IEEE Trans. Power Electron.*, vol. 32, DOI 10.1109/TPEL.2016.2526740, no. 1, pp. 652–667. [Online]. Available: http://ieeexplore.ieee.org/document/7401083/

[3] D. Park and M. K. Zadeh, "Dynamic Modeling and Stability Analysis of Onboard DC Power System for Hybrid Electric Ships," in *2019 IEEE Transportation Electrification Conference and Expo (ITEC)*, DOI 10.1109/ITEC.2019.8790505, pp. 1–6.

[4] M. Hatlehol, D. Park, and M. K. Zadeh, "A Modified Sliding Mode Controller for Active Stabilization of DC Microgrids with Constant Power Load," in *IECON 2019 - 45th Annual Conference of the IEEE Industrial Electronics Society*, vol. 1, DOI 10.1109/IECON.2019.8927773, pp. 4039–4044.

[5] K. Kwon, D. Park, and M. K. Zadeh, "Load Frequency-Based Power Management for Shipboard DC Hybrid Power Systems," in *2020 IEEE 29th International Symposium on Industrial Electronics (ISIE)*, DOI 10.1109/ISIE45063.2020.9152418, pp. 142–147.

[6] M. Malinowski, M. P. Kazmierkowski, and A. M. Trzynadlowski, "A comparative study of control techniques for PWM rectifiers in AC adjustable speed drives," *IEEE Trans. Power Electron.*, vol. 18, DOI 10.1109/TPEL.2003.818871, no. 6, pp. 1390–1396.

[7] J. Hou, J. Sun, and H. F. Hofmann, "Mitigating Power Fluctuations in Electric Ship Propulsion With Hybrid Energy Storage System: Design and Analysis," *IEEE J. Ocean. Eng.*, vol. 43, DOI 10.1109/JOE.2017.2674878, no. 1, pp. 93–107.

[8] M. M. Mardani, M. H. Khooban, A. Masoudian, and T. Dragičević, "Model Predictive Control of DCâDC Converters to Mitigate the Effects of Pulsed Power Loads in Naval DC Microgrids," *IEEE Trans. Ind. Electron.*, vol. 66, DOI 10.1109/TIE.2018.2877191, no. 7, pp. 5676–5685.

[9] Q. Xiao, L. Chen, H. Jia, P. W. Wheeler, and T. Dragičević, "Model Predictive Control for Dual Active Bridge in Naval DC Microgrids Supplying Pulsed Power Loads Featuring Fast Transition and Online

Transformer Current Minimization," *IEEE Trans. Ind. Electron.*, vol. 67, DOI 10.1109/TIE.2019.2934070, no. 6, pp. 5197–5203.
[10] T. V. Vu, D. Gonsoulin, F. Diaz, C. S. Edrington, and T. El-Mezyani, "Predictive Control for Energy Management in Ship Power Systems Under High-Power Ramp Rate Loads," *IEEE Trans. Energy Convers.*, vol. 32, DOI 10.1109/TEC.2017.2692058, no. 2, pp. 788–797.
[11] E. Skjong, J. A. Suul, A. Rygg, T. A. Johansen, and M. Molinas, "System-Wide Harmonic Mitigation in a Diesel-Electric Ship by Model Predictive Control," *IEEE Trans. Ind. Electron.*, vol. 63, DOI 10.1109/TIE.2016.2532845, no. 7, pp. 4008–4019.
[12] S. Skjong and E. Pedersen, "Nonangular MPC-Based Thrust Allocation Algorithm for Marine VesselsâA Study of Optimal Thruster Commands," *IEEE Trans. Transp. Electrification*, vol. 3, DOI 10.1109/TTE.2017.2688183, no. 3, pp. 792–807.
[13] P. Cortés, J. Rodríguez, P. Antoniewicz, and M. Kazmierkowski, "Direct Power Control of an AFE Using Predictive Control," *IEEE Trans. Power Electron.*, vol. 23, DOI 10.1109/TPEL.2008.2002065, no. 5, pp. 2516–2523.
[14] Y. Shan, J. Hu, K. W. Chan, Q. Fu, and J. M. Guerrero, "Model Predictive Control of Bidirectional DCâDC Converters and AC/DC Interlinking ConvertersâA New Control Method for PV-Wind-Battery Microgrids," *IEEE Trans. Sustain. Energy*, vol. 10, DOI 10.1109/TSTE.2018.2873390, no. 4, pp. 1823–1833.
[15] D. E. Quevedo, R. P. Aguilera, M. A. Perez, P. Cortes, and R. Lizana, "Model Predictive Control of an AFE Rectifier With Dynamic References," *IEEE Trans. Power Electron.*, vol. 27, DOI 10.1109/TPEL.2011.2179672, no. 7, pp. 3128–3136.
[16] M. P. Akter, S. Mekhilef, N. M. L. Tan, and H. Akagi, "Modified Model Predictive Control of a Bidirectional ACâDC Converter Based on Lyapunov Function for Energy Storage Systems," *IEEE Trans. Ind. Electron.*, vol. 63, DOI 10.1109/TIE.2015.2478752, no. 2, pp. 704–715.
[17] L. M. A. Caseiro, A. M. S. Mendes, and S. M. A. Cruz, "Dynamically Weighted Optimal Switching Vector Model Predictive Control of Power Converters," *IEEE Trans. Ind. Electron.*, vol. 66, DOI 10.1109/TIE.2018.2829689, no. 2, pp. 1235–1245.
[18] P. J. d. S. Neto, T. A. d. S. Barros, J. P. C. Silveira, E. R. Filho, J. C. Vasquez, and J. M. Guerrero, "Power Management Strategy Based on Virtual Inertia for DC Microgrids," *IEEE Trans. Power Electron.*, vol. 35, DOI 10.1109/TPEL.2020.2986283, no. 11, pp. 12 472–12 485.
[19] W. Sinsukthavorn, E. Ortjohann, A. Mohd, N. Hamsic, and D. Morton, "Control Strategy for Three-/Four-Wire-Inverter-Based Distributed Generation," *IEEE Trans. Ind. Electron.*, vol. 59, DOI 10.1109/TIE.2012.2188871, no. 10, pp. 3890–3899.
[20] C. Sun, G. Joos, and F. Bouffard, "Adaptive Coordination for Power and SoC Limiting Control of Energy Storage in Islanded AC Microgrid with Impact Load," *IEEE Trans. Power Deliv.*, DOI 10.1109/TPWRD.2019.2916034, pp. 1–1.
[21] B. Zahedi, O. C. Nebb, and L. E. Norum, "An isolated bidirectional converter modeling for hybrid electric ship simulations," in *2012 IEEE Transportation Electrification Conference and Expo (ITEC)*, DOI 10.1109/ITEC.2012.6243424, pp. 1–6. IEEE. [Online]. Available: http://ieeexplore.ieee.org/lpdocs/epic03/wrapper.htm?arnumber=6243424
[22] Danfoss, "VACON NX AC Drives Design Guide Hybridization, Accessed on: Jun. 24, 2020. [Online]. Available: http://files.danfoss.com/download/drives/vacon-hybridization-guide-dpd01887a-uk.pdf."
[23] O. Tremblay, L.-A. Dessaint, and A.-I. Dekkiche, "A Generic Battery Model for the Dynamic Simulation of Hybrid Electric Vehicles," in *2007 IEEE Vehicle Power and Propulsion Conference*, DOI 10.1109/VPPC.2007.4544139, pp. 284–289. IEEE. [Online]. Available: http://ieeexplore.ieee.org/document/4544139/
[24] L. W. Y. Chua, T. Tjahjowidodo, G. G. L. Seet, and R. Chan, "Implementation of Optimization-Based Power Management for All-Electric Hybrid Vessels," *IEEE Access*, vol. 6, DOI 10.1109/ACCESS.2018.2883324, pp. 74 339–74 354.
[25] M. B. Othman, N. P. Reddy, P. Ghimire, M. K. Zadeh, A. Anvari-Moghaddam, and J. M. Guerrero, "A Hybrid Power System Laboratory: Testing Electric and Hybrid Propulsion," *IEEE Electrification Mag.*, vol. 7, DOI 10.1109/MELE.2019.2943982, no. 4, pp. 89–97.

Daeseong Park was born in Seoul, Republic of Korea, in 1987. He received the B.Sc.degree in naval architecture and ocean engineering with Cum Laude from Seoul National University, Republic of Korea, in 2013, and the M.Sc. degree in Marine Technology from the Norwegian University of Science and Technology (NTNU), Trondheim, Norway, in 2018. He is currently working toward the Ph.D. degree in the Department of Marine Technology at NTNU. He worked as an assistant engineer for ship systems in Daewoo Shipbuilding and Marine Engineering (DSME) from 2013 to 2016. His current research interests include modeling, control and stability analysis of shipboard power systems.

Mehdi Zadeh received the Ph.D. degree in Electrical Engineering from NTNU, Trondheim, Norway, in 2016. From 2016 to 2017, he was with the power electronics industry, working on the development of battery charging systems. In 2017, he joined the Marine Technology Centre at NTNU in Trondheim, where he is currently an Associate Professor of Hybrid Power Systems and the director of the Marine Electrification Research Lab. His main research interests include ship electrification for low-emission and autonomous shipping, onboard DC power systems, and offshore renewable energy systems.